IEEE Access
Multidisciplinary | Rapid Review | Open Access Journal

Received October 22, 2017, accepted November 19, 2017, date of publication November 27, 2017,
date of current version December 22, 2017.

Digital Object Identifier 10.1109/ACCESS.2017.2777818

3-D Reconstruction of Binocular Vision Using Distance Objective Generated From Two Pairs of Skew Projection Lines

GUAN XU[1], (Member, IEEE), JUNYI CHEN[1], AND XIAOTAO LI[2]
[1]Department of Vehicle Operation Engineering, Traffic and Transportation College, Jilin University, Changchun 130025, China
[2]School of Mechanical Science and Engineering, Nanling Campus, Jilin University, Changchun 130025, China

Corresponding author: Xiaotao Li (lixiaotao@jlu.edu.cn)

The work was supported in part by the National Natural Science Foundation of China under Grant 51478204 and Grant 51205164, and in part by the Natural Science Foundation of Jilin Province under Grant 20170101214JC and Grant 20150101027JC.

ABSTRACT A reconstruction method is provided to improve the measurement of the binocular vision. The image projections of the 3-D point on the 3-D reference are analyzed by the multiple view geometry. The Plücker coordinates of the two screw projection lines are constructed by the image points. The line segment perpendicular to two projection lines is generated from the direction vector and the end points of the line segment. As the bilinear products of the Plücker coordinates between the perpendicular line and the projection lines are zero, the end points of the perpendicular line segment are parameterized by the Cramer's Rule. The reconstruction error of the distance between two parameterized 3-D points is employed as the minimized objective of the cost function. The impact factors and the enhancements of the reconstruction accuracy are investigated by the experiments comparing with the original method. The method contributes the error descents of 27.19%, 38.29%, 19.01%,and 16.31% for the test lengths of 50, 100, 150, and 200 mm. Therefore, the results demonstrate that reconstruction method of the binocular vision provides the higher accuracy and application potentials.

INDEX TERMS Binocular vision, calibration, 3D reconstruction.

I. INTRODUCTION

Vision-based measurement is an important aspect of the optical detection, due to the advantages of non-touch measurement, low cost and capability of spatial inspection [1]–[3]. It has been widely studied in the typical application fields of vehicle navigation [4], robots [5], [6], medical operation [7] and architecture [8], etc.

Two majors of the vision-based measurement are reported in previous works. The first method is the monocular vision, which employs one camera to perform the measurement task [9]. The projection from the object to the image plane is described by the intrinsic and extrinsic parameters of the camera. Furthermore, the spatial information can be conditionally recovered by the captured object image. In the monocular vision, the intrinsic and extrinsic parameters of the camera are derived from the calibration process with the 1D [2], [10], 2D [11]–[14] and 3D [15], [16] references. As the projection from the 3D object to the 2D image loses a dimension, only the homography information from the 2D plane to the 2D image is reserved in the monocular vision. Therefore, the 3D reconstruction of the monocular vision is limited to the coplanar points on the basic plane of the world coordinate system. In addition, three or more images are required to realize the 3D reconstruction [17]. In order to improve the 3D reconstruction, the binocular vision is proposed to acquire the entire 3D object information [18]. There are also two branches in the binocular vision. The first is that one camera captures two images of the same object [19]. The second is that two cameras capture two images of the object [20]. The first approach depends on the relative motion between the camera and the object. The essential matrix is generated from the trianglarity to reconstruct the 3D object. The extrinsic parameters can be decomposed from the essential matrix. The first binocular approach relies on the appropriate baseline and the measurement result is up to a scale factor [21]. The second approach adopting the two cameras benefits from the fixed baseline between the two cameras. The 3D measurement is achieved from the calibration of the binocular vision system. The reconstruction accuracy of the binocular system with the short baseline is easy to be impacted by the noises in

the images, while the long baseline also takes the problem of matching difficulty, even employing the robust method of the scale-invariant feature transform (SIFT) [22]. Therefore, the relationship between the reconstruction accuracy and the baseline length is valuable for a measurement method of the binocular system.

The 3D reconstruction is generated from the calibration results, which depends on the features of the point, the line, the circle [23], etc. As the lines and the circles provide the smaller amount of features than the points, the point-based calibration is widely used in the calibration process. In the paper, a reconstruction method is provided with the optimization objective of the distance between the spatial benchmark points, which is different from the former method with the optimization objective of the point reprojection errors and the epipolar constraint [24]. The 3D reference is employed due to the higher calibration accuracy than 1D and 2D references. The rest article is organized as follows: In Section 2, the projection geometry of the binocular vision is analyzed and the parameterized distance of the spatial points is generated from the bilinear products of the Plücker coordinates and the Cramer's Rule. In Section 3, the reconstruction method is verified by the comprehensive experiments, under different measurement distances, different baseline distances and different test lengths. Section 4 summarizes the paper.

II. RECONSTRUCTION METHOD

The calibration approach for the binocular vision system is illustrated in Fig. 1. The 3D reference is employed to calibrate the system parameters of the binocular system. The world coordinate system O-XYZ is defined by the 3D reference. Two camera coordinate systems $O_1 - X_1Y_1Z_1$, $O_2 - X_2Y_2Z_2$ are determined by the two cameras of the binocular vision system. The image coordinate systems are generated from two images. A 3D corner point $\mathbf{X}_i$ is projected to two images by two cameras.

The reconstruction method consists of four main parts. First, two skew projection lines are generated from the projection process and represented by the Plücker coordinates. Then, the direction vector of the perpendicular line of the two projection lines is solved by the Plücker coordinates. Third, the parameterized 3D point is obtained from the bilinear products among the Plücker coordinates of the two projection lines and the common perpendicular line. Finally, the projection matrices are optimized by minimizing the reconstruction error of the distance between two adjacent corner points on the 3D reference.

The projection points of $\mathbf{X}_i$ are $\mathbf{x}_i^{\mathrm{I}}$ $\mathbf{x}_i^{\mathrm{II}}$ in the two images. The projections are expressed as [25]:

$$\mathrm{P}^{\mathrm{I}}\mathbf{X}_i = s_1\mathbf{x}_i^{\mathrm{I}} \tag{1}$$

$$\mathrm{P}^{\mathrm{II}}\mathbf{X}_i = s_2\mathbf{x}_i^{\mathrm{II}} \tag{2}$$

where $\mathrm{P}^{\mathrm{I}} = [p^{\mathrm{I}}_{\alpha,\beta}]_{3\times4}$, $\mathrm{P}^{\mathrm{II}} = [p^{\mathrm{II}}_{\alpha,\beta}]_{3\times4}$ are the projection matrices of the two cameras. $\mathbf{x}_i^{\mathrm{I}} = [x_i^{\mathrm{I}}, y_i^{\mathrm{I}}, 1]^{\mathrm{T}}$, $\mathbf{x}_i^{\mathrm{II}} = [x_i^{\mathrm{II}}, y_i^{\mathrm{II}}, 1]^{\mathrm{T}}$ are the projection points of $\mathbf{X}_i = [X_i, Y_i, Z_i, 1]^{\mathrm{T}}$. s_1 and s_2 are two scale factors.

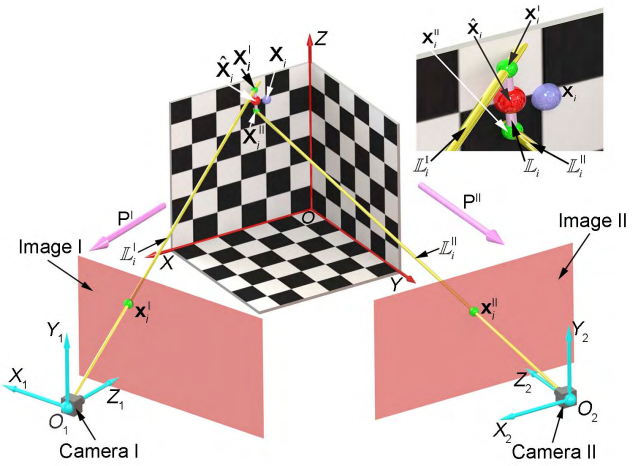

FIGURE 1. Parameterization method of the 3D point on the reference.

Equations. (1) and (2) are transformed to [21], [26]:

$$\begin{aligned}
&(p^{\mathrm{I}}_{11} - p^{\mathrm{I}}_{31}x^{\mathrm{I}}_i)X_i + (p^{\mathrm{I}}_{12} - p^{\mathrm{I}}_{32}x^{\mathrm{I}}_i)Y_i \\
&\qquad + (p^{\mathrm{I}}_{13} - p^{\mathrm{I}}_{33}x^{\mathrm{I}}_i)Z_i + p^{\mathrm{I}}_{14} - p^{\mathrm{I}}_{34}x^{\mathrm{I}}_i = 0 \\
&(p^{\mathrm{I}}_{21} - p^{\mathrm{I}}_{31}y^{\mathrm{I}}_i)X_i + (p^{\mathrm{I}}_{22} - p^{\mathrm{I}}_{32}y^{\mathrm{I}}_i)Y_i \\
&\qquad + (p^{\mathrm{I}}_{23} - p^{\mathrm{I}}_{33}y^{\mathrm{I}}_i)Z_i + p^{\mathrm{I}}_{24} - p^{\mathrm{I}}_{34}y^{\mathrm{I}}_i = 0
\end{aligned} \tag{3}$$

$$\begin{aligned}
&(p^{\mathrm{II}}_{11} - p^{\mathrm{II}}_{31}x^{\mathrm{II}}_i)X_i + (p^{\mathrm{II}}_{12} - p^{\mathrm{II}}_{32}x^{\mathrm{II}}_i)Y_i \\
&\qquad + (p^{\mathrm{II}}_{13} - p^{\mathrm{II}}_{33}x^{\mathrm{II}}_i)Z_i + p^{\mathrm{II}}_{14} - p^{\mathrm{II}}_{34}x^{\mathrm{II}}_i = 0 \\
&(p^{\mathrm{II}}_{21} - p^{\mathrm{II}}_{31}y^{\mathrm{II}}_i)X_i + (p^{\mathrm{II}}_{22} - p^{\mathrm{II}}_{32}y^{\mathrm{II}}_i)Y_i \\
&\qquad + (p^{\mathrm{II}}_{23} - p^{\mathrm{II}}_{33}y^{\mathrm{II}}_i)Z_i + p^{\mathrm{II}}_{24} - p^{\mathrm{II}}_{34}y^{\mathrm{II}}_i = 0
\end{aligned} \tag{4}$$

Two equations in Eq. (3) or Eq. (4) represent an intersection line of two planes. Thus, the intersection point of the two intersection lines in Eqs. (3) and (4) stands for the 3D corner point $\mathbf{X}_i$, theoretically.

As the noises impact on the positions of the projection points $\mathbf{x}_i^{\mathrm{I}}$, $\mathbf{x}_i^{\mathrm{II}}$, the projection lines of the two projection points do not intersect at the 3D corner point $\mathbf{X}_i$, actually. In other words, the projection lines of the projection points are two screw lines.

According to Eqs. (3) and (4), the Plücker matrices of the two projection lines are expressed as:

$$\begin{aligned}
\mathrm{L}_i^{*\mathrm{I}} &= (\mathrm{R}_i^{\mathrm{I}})(\mathrm{Q}_i^{\mathrm{I}})^{\mathrm{T}} - (\mathrm{Q}_i^{\mathrm{I}})(\mathrm{R}_i^{\mathrm{I}})^{\mathrm{T}} \\
&= \begin{bmatrix}
0 & (l_i^*)^{\mathrm{I}}_{12} & (l_i^*)^{\mathrm{I}}_{13} & (l_i^*)^{\mathrm{I}}_{14} \\
(l_i^*)^{\mathrm{I}}_{21} & 0 & (l_i^*)^{\mathrm{I}}_{23} & (l_i^*)^{\mathrm{I}}_{24} \\
(l_i^*)^{\mathrm{I}}_{31} & (l_i^*)^{\mathrm{I}}_{32} & 0 & (l_i^*)^{\mathrm{I}}_{34} \\
(l_i^*)^{\mathrm{I}}_{41} & (l_i^*)^{\mathrm{I}}_{42} & (l_i^*)^{\mathrm{I}}_{43} & 0
\end{bmatrix}
\end{aligned} \tag{5}$$

$$\begin{aligned}
\mathrm{L}_i^{*\mathrm{II}} &= (\mathrm{R}_i^{\mathrm{II}})(\mathrm{Q}_i^{\mathrm{II}})^{\mathrm{T}} - (\mathrm{Q}_i^{\mathrm{II}})(\mathrm{R}_i^{\mathrm{II}})^{\mathrm{T}} \\
&= \begin{bmatrix}
0 & (l_i^*)^{\mathrm{II}}_{12} & (l_i^*)^{\mathrm{II}}_{13} & (l_i^*)^{\mathrm{II}}_{14} \\
(l_i^*)^{\mathrm{II}}_{21} & 0 & (l_i^*)^{\mathrm{II}}_{23} & (l_i^*)^{\mathrm{II}}_{24} \\
(l_i^*)^{\mathrm{II}}_{31} & (l_i^*)^{\mathrm{II}}_{32} & 0 & (l_i^*)^{\mathrm{II}}_{34} \\
(l_i^*)^{\mathrm{II}}_{41} & (l_i^*)^{\mathrm{II}}_{42} & (l_i^*)^{\mathrm{II}}_{43} & 0
\end{bmatrix}
\end{aligned} \tag{6}$$

where

$$\begin{aligned}
\mathrm{R}_i^{\mathrm{I}} &= [(p_{11}^{\mathrm{I}} - p_{31}^{\mathrm{I}}x_i^{\mathrm{I}}), (p_{12}^{\mathrm{I}} - p_{32}^{\mathrm{I}}x_i^{\mathrm{I}}),\\
&\quad (p_{13}^{\mathrm{I}} - p_{33}^{\mathrm{I}}x_i^{\mathrm{I}}), (p_{14}^{\mathrm{I}} - p_{34}^{\mathrm{I}}x_i^{\mathrm{I}})]^{\mathrm{T}},\\
\mathrm{Q}_i^{\mathrm{I}} &= [(p_{21}^{\mathrm{I}} - p_{31}^{\mathrm{I}}y_i^{\mathrm{I}}), (p_{22}^{\mathrm{I}} - p_{32}^{\mathrm{I}}y_i^{\mathrm{I}}),\\
&\quad (p_{23}^{\mathrm{I}} - p_{33}^{\mathrm{I}}y_i^{\mathrm{I}}), (p_{24}^{\mathrm{I}} - p_{34}^{\mathrm{I}}y_i^{\mathrm{I}})]^{\mathrm{T}},\\
\mathrm{R}_i^{\mathrm{II}} &= [(p_{11}^{\mathrm{II}} - p_{31}^{\mathrm{II}}x_i^{\mathrm{II}}), (p_{12}^{\mathrm{II}} - p_{32}^{\mathrm{II}}x_i^{\mathrm{II}}),\\
&\quad (p_{13}^{\mathrm{II}} - p_{33}^{\mathrm{II}}x_i^{\mathrm{II}}), (p_{14}^{\mathrm{II}} - p_{34}^{\mathrm{II}}x_i^{\mathrm{II}})]^{\mathrm{T}}
\end{aligned}$$

and

$$\begin{aligned}
\mathrm{Q}_i^{\mathrm{II}} &= [(p_{21}^{\mathrm{II}} - p_{31}^{\mathrm{II}}y_i^{\mathrm{II}}), (p_{22}^{\mathrm{II}} - p_{32}^{\mathrm{II}}y_i^{\mathrm{II}}),\\
&\quad (p_{23}^{\mathrm{II}} - p_{33}^{\mathrm{II}}y_i^{\mathrm{II}}), (p_{24}^{\mathrm{II}} - p_{34}^{\mathrm{II}}y_i^{\mathrm{II}})]^{\mathrm{T}}
\end{aligned}$$

are the four planes in Eqs. (3) and (4).

From Eqs. (5) , (6) and the dual relationship of $(l_{34}^*)^{\mathrm{I,II}} : (l_{42}^*)^{\mathrm{I,II}} : (l_{23}^*)^{\mathrm{I,II}} : (l_{14}^*)^{\mathrm{I,II}} : (l_{13}^*)^{\mathrm{I,II}} : (l_{12}^*)^{\mathrm{I,II}} = (l_{12})^{\mathrm{I,II}} : (l_{13})^{\mathrm{I,II}} : (l_{14})^{\mathrm{I,II}} : (l_{23})^{\mathrm{I,II}} : (l_{42})^{\mathrm{I,II}} : (l_{34})^{\mathrm{I,II}}$ [26] the Plücker coordinates of the two projection lines are given as:

$$\mathrm{L}_i^{\mathrm{I}} = \left\{(l_i)_{12}^{\mathrm{I}}, (l_i)_{13}^{\mathrm{I}}, (l_i)_{14}^{\mathrm{I}}, (l_i)_{23}^{\mathrm{I}}, (l_i)_{42}^{\mathrm{I}}, (l_i)_{34}^{\mathrm{I}}\right\} \tag{7}$$

$$\mathrm{L}_i^{\mathrm{II}} = \left\{(l_i)_{12}^{\mathrm{II}}, (l_i)_{13}^{\mathrm{II}}, (l_i)_{14}^{\mathrm{II}}, (l_i)_{23}^{\mathrm{II}}, (l_i)_{42}^{\mathrm{II}}, (l_i)_{34}^{\mathrm{II}}\right\} \tag{8}$$

where

$$\begin{aligned}
(l_i)_{12}^{\mathrm{I}} &= (p_{13}^{\mathrm{I}} - p_{33}^{\mathrm{I}}x_i^{\mathrm{I}})(p_{24}^{\mathrm{I}} - p_{34}^{\mathrm{I}}y_i^{\mathrm{I}})\\
&\quad - (p_{23}^{\mathrm{I}} - p_{33}^{\mathrm{I}}y_i^{\mathrm{I}})(p_{14}^{\mathrm{I}} - p_{34}^{\mathrm{I}}x_i^{\mathrm{I}}),\\
(l_i)_{13}^{\mathrm{I}} &= (p_{14}^{\mathrm{I}} - p_{34}^{\mathrm{I}}x_i^{\mathrm{I}})(p_{22}^{\mathrm{I}} - p_{32}^{\mathrm{I}}y_i^{\mathrm{I}})\\
&\quad - (p_{24}^{\mathrm{I}} - p_{34}^{\mathrm{I}}y_i^{\mathrm{I}})(p_{12}^{\mathrm{I}} - p_{32}^{\mathrm{I}}x_i^{\mathrm{I}}),\\
(l_i)_{14}^{\mathrm{I}} &= (p_{12}^{\mathrm{I}} - p_{32}^{\mathrm{I}}x_i^{\mathrm{I}})(p_{23}^{\mathrm{I}} - p_{33}^{\mathrm{I}}y_i^{\mathrm{I}})\\
&\quad - (p_{22}^{\mathrm{I}} - p_{32}^{\mathrm{I}}y_i^{\mathrm{I}})(p_{13}^{\mathrm{I}} - p_{33}^{\mathrm{I}}x_i^{\mathrm{I}}),\\
(l_i)_{23}^{\mathrm{I}} &= (p_{11}^{\mathrm{I}} - p_{31}^{\mathrm{I}}x_i^{\mathrm{I}})(p_{24}^{\mathrm{I}} - p_{34}^{\mathrm{I}}y_i^{\mathrm{I}})\\
&\quad - (p_{21}^{\mathrm{I}} - p_{31}^{\mathrm{I}}y_i^{\mathrm{I}})(p_{14}^{\mathrm{I}} - p_{34}^{\mathrm{I}}x_i^{\mathrm{I}}),\\
(l_i)_{42}^{\mathrm{I}} &= (p_{11}^{\mathrm{I}} - p_{31}^{\mathrm{I}}x_i^{\mathrm{I}})(p_{23}^{\mathrm{I}} - p_{33}^{\mathrm{I}}y_i^{\mathrm{I}})\\
&\quad - (p_{21}^{\mathrm{I}} - p_{31}^{\mathrm{I}}y_i^{\mathrm{I}})(p_{13}^{\mathrm{I}} - p_{33}^{\mathrm{I}}x_i^{\mathrm{I}}),\\
(l_i)_{34}^{\mathrm{I}} &= (p_{11}^{\mathrm{I}} - p_{31}^{\mathrm{I}}x_i^{\mathrm{I}})(p_{22}^{\mathrm{I}} - p_{32}^{\mathrm{I}}y_i^{\mathrm{I}})\\
&\quad - (p_{21}^{\mathrm{I}} - p_{31}^{\mathrm{I}}y_i^{\mathrm{I}})(p_{12}^{\mathrm{I}} - p_{32}^{\mathrm{I}}x_i^{\mathrm{I}}),\\
(l_i)_{12}^{\mathrm{II}} &= (p_{13}^{\mathrm{II}} - p_{33}^{\mathrm{II}}x_i^{\mathrm{II}})(p_{24}^{\mathrm{II}} - p_{34}^{\mathrm{II}}y_i^{\mathrm{II}})\\
&\quad - (p_{23}^{\mathrm{II}} - p_{33}^{\mathrm{II}}y_i^{\mathrm{II}})(p_{14}^{\mathrm{II}} - p_{34}^{\mathrm{II}}x_i^{\mathrm{II}}),\\
(l_i)_{13}^{\mathrm{II}} &= (p_{14}^{\mathrm{II}} - p_{34}^{\mathrm{II}}x_i^{\mathrm{II}})(p_{22}^{\mathrm{II}} - p_{32}^{\mathrm{II}}y_i^{\mathrm{II}})\\
&\quad - (p_{24}^{\mathrm{II}} - p_{34}^{\mathrm{II}}y_i^{\mathrm{II}})(p_{12}^{\mathrm{II}} - p_{32}^{\mathrm{II}}x_i^{\mathrm{II}}),\\
(l_i)_{14}^{\mathrm{II}} &= (p_{12}^{\mathrm{II}} - p_{32}^{\mathrm{II}}x_i^{\mathrm{II}})(p_{23}^{\mathrm{II}} - p_{33}^{\mathrm{II}}y_i^{\mathrm{II}})\\
&\quad - (p_{22}^{\mathrm{II}} - p_{32}^{\mathrm{II}}y_i^{\mathrm{II}})(p_{13}^{\mathrm{II}} - p_{33}^{\mathrm{II}}x_i^{\mathrm{II}}),\\
(l_i)_{23}^{\mathrm{II}} &= (p_{11}^{\mathrm{II}} - p_{31}^{\mathrm{II}}x_i^{\mathrm{II}})(p_{24}^{\mathrm{II}} - p_{34}^{\mathrm{II}}y_i^{\mathrm{II}})\\
&\quad - (p_{21}^{\mathrm{II}} - p_{31}^{\mathrm{II}}y_i^{\mathrm{II}})(p_{14}^{\mathrm{II}} - p_{34}^{\mathrm{II}}x_i^{\mathrm{II}}),\\
(l_i)_{42}^{\mathrm{II}} &= (p_{11}^{\mathrm{II}} - p_{31}^{\mathrm{II}}x_i^{\mathrm{II}})(p_{23}^{\mathrm{II}} - p_{33}^{\mathrm{II}}y_i^{\mathrm{II}})\\
&\quad - (p_{21}^{\mathrm{II}} - p_{31}^{\mathrm{II}}y_i^{\mathrm{II}})(p_{13}^{\mathrm{II}} - p_{33}^{\mathrm{II}}x_i^{\mathrm{II}}),\\
(l_i)_{34}^{\mathrm{II}} &= (p_{11}^{\mathrm{II}} - p_{31}^{\mathrm{II}}x_i^{\mathrm{II}})(p_{22}^{\mathrm{II}} - p_{32}^{\mathrm{II}}y_i^{\mathrm{II}})\\
&\quad - (p_{21}^{\mathrm{II}} - p_{31}^{\mathrm{II}}y_i^{\mathrm{II}})(p_{12}^{\mathrm{II}} - p_{32}^{\mathrm{II}}x_i^{\mathrm{II}}).
\end{aligned}$$

In order to solve the direction vector of the perpendicular line segment of the two projection lines, the direction vectors of the intersection lines are [27]:

$$\begin{aligned}
&\mathbf{u}_i^{\mathrm{I}}\\
&= \mathbf{m}_i^{\mathrm{I}} \times \mathbf{n}_i^{\mathrm{I}}\\
&= \begin{bmatrix}(p_{12}^{\mathrm{I}} - p_{32}^{\mathrm{I}}x_i^{\mathrm{I}})(p_{23}^{\mathrm{I}} - p_{33}^{\mathrm{I}}y_i^{\mathrm{I}}) - (p_{13}^{\mathrm{I}} - p_{33}^{\mathrm{I}}x_i^{\mathrm{I}})(p_{22}^{\mathrm{I}} - p_{32}^{\mathrm{I}}y_i^{\mathrm{I}})\\ (p_{13}^{\mathrm{I}} - p_{33}^{\mathrm{I}}x_i^{\mathrm{I}})(p_{21}^{\mathrm{I}} - p_{31}^{\mathrm{I}}y_i^{\mathrm{I}}) - (p_{11}^{\mathrm{I}} - p_{31}^{\mathrm{I}}x_i^{\mathrm{I}})(p_{23}^{\mathrm{I}} - p_{33}^{\mathrm{I}}y_i^{\mathrm{I}})\\ (p_{11}^{\mathrm{I}} - p_{31}^{\mathrm{I}}x_i^{\mathrm{I}})(p_{22}^{\mathrm{I}} - p_{32}^{\mathrm{I}}y_i^{\mathrm{I}}) - (p_{13}^{\mathrm{I}} - p_{33}^{\mathrm{I}}x_i^{\mathrm{I}})(p_{21}^{\mathrm{I}} - p_{31}^{\mathrm{I}}y_i^{\mathrm{I}})\end{bmatrix}
\end{aligned} \tag{9}$$

$$\begin{aligned}
&\mathbf{u}_i^{\mathrm{II}}\\
&= \mathbf{m}_i^{\mathrm{II}} \times \mathbf{n}_i^{\mathrm{II}}\\
&= \begin{bmatrix}(p_{12}^{\mathrm{II}} - p_{32}^{\mathrm{II}}x_i^{\mathrm{II}})(p_{23}^{\mathrm{II}} - p_{33}^{\mathrm{II}}y_i^{\mathrm{II}}) - (p_{13}^{\mathrm{II}} - p_{33}^{\mathrm{II}}x_i^{\mathrm{II}})(p_{22}^{\mathrm{II}} - p_{32}^{\mathrm{II}}y_i^{\mathrm{II}})\\ (p_{13}^{\mathrm{II}} - p_{33}^{\mathrm{II}}x_i^{\mathrm{II}})(p_{21}^{\mathrm{II}} - p_{31}^{\mathrm{II}}y_i^{\mathrm{II}}) - (p_{11}^{\mathrm{II}} - p_{31}^{\mathrm{II}}x_i^{\mathrm{II}})(p_{23}^{\mathrm{II}} - p_{33}^{\mathrm{II}}y_i^{\mathrm{II}})\\ (p_{11}^{\mathrm{II}} - p_{31}^{\mathrm{II}}x_i^{\mathrm{II}})(p_{22}^{\mathrm{II}} - p_{32}^{\mathrm{II}}y_i^{\mathrm{II}}) - (p_{13}^{\mathrm{II}} - p_{33}^{\mathrm{II}}x_i^{\mathrm{II}})(p_{21}^{\mathrm{II}} - p_{31}^{\mathrm{II}}y_i^{\mathrm{II}})\end{bmatrix}
\end{aligned} \tag{10}$$

where

$$\begin{aligned}
\mathbf{n}_i^{\mathrm{I}} &= [(p_{11}^{\mathrm{I}} - p_{31}^{\mathrm{I}}x_i^{\mathrm{I}}), (p_{12}^{\mathrm{I}} - p_{32}^{\mathrm{I}}x_i^{\mathrm{I}}), (p_{13}^{\mathrm{I}} - p_{33}^{\mathrm{I}}x_i^{\mathrm{I}})]^{\mathrm{T}},\\
\mathbf{m}_i^{\mathrm{I}} &= [(p_{21}^{\mathrm{I}} - p_{31}^{\mathrm{I}}y_i^{\mathrm{I}}), (p_{22}^{\mathrm{I}} - p_{32}^{\mathrm{I}}y_i^{\mathrm{I}}), (p_{23}^{\mathrm{I}} - p_{33}^{\mathrm{I}}y_i^{\mathrm{I}})]^{\mathrm{T}},\\
\mathbf{n}_i^{\mathrm{II}} &= [(p_{11}^{\mathrm{II}} - p_{31}^{\mathrm{II}}x_i^{\mathrm{II}}), (p_{12}^{\mathrm{I\,I}} - p_{32}^{\mathrm{II}}x_i^{\mathrm{II}}), (p_{13}^{\mathrm{II}} - p_{33}^{\mathrm{II}}x_i^{\mathrm{II}})]^{\mathrm{T}},\\
\mathbf{m}_i^{\mathrm{II}} &= [(p_{21}^{\mathrm{II}} - p_{31}^{\mathrm{II}}y_i^{\mathrm{II}}), (p_{22}^{\mathrm{I\,I}} - p_{32}^{\mathrm{II}}y_i^{\mathrm{II}}), (p_{23}^{\mathrm{II}} - p_{33}^{\mathrm{II}}y_i^{\mathrm{II}})]^{\mathrm{T}}.
\end{aligned}$$

Therefore, the normal vector to the intersection lines is [27]:

$$\mathbf{v}_i = \mathbf{u}_i^{\mathrm{I}} \times \mathbf{u}_i^{\mathrm{II}} = [v_{xi}, v_{yi}, v_{zi}]^{\mathrm{T}} \tag{11}$$

where

$$\begin{aligned}
v_{xi} &= \left[(p_{13}^{\mathrm{I}} - p_{33}^{\mathrm{I}}x_i^{\mathrm{I}})(p_{21}^{\mathrm{I}} - p_{31}^{\mathrm{I}}y_i^{\mathrm{I}}) - (p_{11}^{\mathrm{I}} - p_{31}^{\mathrm{I}}x_i^{\mathrm{I}})(p_{23}^{\mathrm{I}}\right.\\
&\quad \left. - p_{33}^{\mathrm{I}}y_i^{\mathrm{I}})\right]\left[(p_{11}^{\mathrm{II}} - p_{31}^{\mathrm{II}}x_i^{\mathrm{II}})(p_{22}^{\mathrm{II}} - p_{32}^{\mathrm{II}}y_i^{\mathrm{II}})\right.\\
&\quad \left. - (p_{13}^{\mathrm{II}} - p_{33}^{\mathrm{II}}x_i^{\mathrm{II}})(p_{21}^{\mathrm{II}} - p_{31}^{\mathrm{II}}y_i^{\mathrm{II}})\right]\\
&\quad - \left[(p_{11}^{\mathrm{I}} - p_{31}^{\mathrm{I}}x_i^{\mathrm{I}})(p_{22}^{\mathrm{I}} - p_{32}^{\mathrm{I}}y_i^{\mathrm{I}}) - (p_{13}^{\mathrm{I}} - p_{33}^{\mathrm{I}}x_i^{\mathrm{I}})(p_{21}^{\mathrm{I}}\right.\\
&\quad \left. - p_{31}^{\mathrm{I}}y_i^{\mathrm{I}})\right]\left[(p_{13}^{\mathrm{II}} - p_{33}^{\mathrm{II}}x_i^{\mathrm{II}})(p_{21}^{\mathrm{II}} - p_{31}^{\mathrm{II}}y_i^{\mathrm{II}})\right.\\
&\quad \left. - (p_{11}^{\mathrm{II}} - p_{31}^{\mathrm{II}}x_i^{\mathrm{II}})(p_{23}^{\mathrm{II}} - p_{33}^{\mathrm{II}}y_i^{\mathrm{II}})\right],\\
v_{yi} &= \left[(p_{11}^{\mathrm{I}} - p_{31}^{\mathrm{I}}x_i^{\mathrm{I}})(p_{22}^{\mathrm{I}} - p_{32}^{\mathrm{I}}y_i^{\mathrm{I}}) - (p_{13}^{\mathrm{I}} - p_{33}^{\mathrm{I}}x_i^{\mathrm{I}})(p_{21}^{\mathrm{I}}\right.\\
&\quad \left. - p_{31}^{\mathrm{I}}y_i^{\mathrm{I}})\right]\left[(p_{12}^{\mathrm{II}} - p_{32}^{\mathrm{II}}x_i^{\mathrm{II}})(p_{23}^{\mathrm{II}} - p_{33}^{\mathrm{II}}y_i^{\mathrm{II}})\right.\\
&\quad \left. - (p_{13}^{\mathrm{II}} - p_{33}^{\mathrm{II}}x_i^{\mathrm{II}})(p_{22}^{\mathrm{II}} - p_{32}^{\mathrm{II}}y_i^{\mathrm{II}})\right]\\
&\quad - \left[(p_{12}^{\mathrm{I}} - p_{32}^{\mathrm{I}}x_i^{\mathrm{I}})(p_{23}^{\mathrm{I}} - p_{33}^{\mathrm{I}}y_i^{\mathrm{I}}) - (p_{13}^{\mathrm{I}} - p_{33}^{\mathrm{I}}x_i^{\mathrm{I}})(p_{22}^{\mathrm{I}}\right.\\
&\quad \left. - p_{32}^{\mathrm{I}}y_i^{\mathrm{I}})\right]\left[(p_{11}^{\mathrm{II}} - p_{31}^{\mathrm{II}}x_i^{\mathrm{II}})(p_{22}^{\mathrm{II}} - p_{32}^{\mathrm{II}}y_i^{\mathrm{II}})\right.\\
&\quad \left. - (p_{13}^{\mathrm{II}} - p_{33}^{\mathrm{II}}x_i^{\mathrm{II}})(p_{21}^{\mathrm{II}} - p_{31}^{\mathrm{II}}y_i^{\mathrm{II}})\right],\\
v_{zi} &= \left[(p_{12}^{\mathrm{I}} - p_{32}^{\mathrm{I}}x_i^{\mathrm{I}})(p_{23}^{\mathrm{I}} - p_{33}^{\mathrm{I}}y_i^{\mathrm{I}}) - (p_{13}^{\mathrm{I}} - p_{33}^{\mathrm{I}}x_i^{\mathrm{I}})(p_{22}^{\mathrm{I}}\right.\\
&\quad \left. - p_{32}^{\mathrm{I}}y_i^{\mathrm{I}})\right]\left[(p_{13}^{\mathrm{II}} - p_{33}^{\mathrm{II}}x_i^{\mathrm{II}})(p_{21}^{\mathrm{II}} - p_{31}^{\mathrm{II}}y_i^{\mathrm{II}})\right.\\
&\quad \left. - (p_{11}^{\mathrm{II}} - p_{31}^{\mathrm{II}}x_i^{\mathrm{II}})(p_{23}^{\mathrm{II}} - p_{33}^{\mathrm{II}}y_i^{\mathrm{II}})\right]
\end{aligned}$$

$$-\left[(p_{13}^{\mathrm{I}}-p_{33}^{\mathrm{I}}x_i^{\mathrm{I}})(p_{21}^{\mathrm{I}}-p_{31}^{\mathrm{I}}y_i^{\mathrm{I}})-(p_{11}^{\mathrm{I}}-p_{31}^{\mathrm{I}}x_i^{\mathrm{I}})(p_{23}^{\mathrm{I}}-p_{33}^{\mathrm{I}}y_i^{\mathrm{I}})\right]\left[(p_{12}^{\mathrm{II}}-p_{32}^{\mathrm{II}}x_i^{\mathrm{II}})(p_{23}^{\mathrm{II}}-p_{33}^{\mathrm{II}}y_i^{\mathrm{II}})-(p_{13}^{\mathrm{II}}-p_{33}^{\mathrm{II}}x_i^{\mathrm{II}})(p_{22}^{\mathrm{II}}-p_{32}^{\mathrm{II}}y_i^{\mathrm{II}})\right].$$

Let the end points of the line segment perpendicular to the two projection lines be $\mathbf{X}_i^{\mathrm{I}} = [X_i^{\mathrm{I}}, Y_i^{\mathrm{I}}, Z_i^{\mathrm{I}}, 1]^{\mathrm{T}}$, $\mathbf{X}_i^{\mathrm{II}} = [X_i^{\mathrm{II}}, Y_i^{\mathrm{II}}, Z_i^{\mathrm{II}}, 1]^{\mathrm{T}}$. The perpendicular line of the two projection lines is:

$$\begin{aligned} v_{yi}X^{\mathrm{I}} - v_{xi}Y^{\mathrm{I}} + v_{xi}Y_i^{\mathrm{I}} - v_{yi}X_i^{\mathrm{I}} &= 0 \\ v_{zi}X^{\mathrm{I}} - v_{xi}Z^{\mathrm{I}} + v_{xi}Z_i^{\mathrm{I}} - v_{zi}X_i^{\mathrm{I}} &= 0 \end{aligned} \tag{12}$$

From Eq. (12), the Plücker matrix of the perpendicular line is:

$$\mathrm{L}_i^* = \mathrm{G}_i(\mathrm{H}_i)^{\mathrm{T}} - \mathrm{H}_i(\mathrm{G}_i)^{\mathrm{T}} = \begin{bmatrix} 0 & l_{12}^* & l_{13}^* & l_{14}^* \\ l_{21}^* & 0 & l_{23}^* & l_{24}^* \\ l_{31}^* & l_{32}^* & 0 & l_{34}^* \\ l_{41}^* & l_{42}^* & l_{43}^* & 0 \end{bmatrix} \tag{13}$$

where $\mathrm{G}_i = [v_{yi}, -v_{xi}, 0, (v_{xi}Y_i^{\mathrm{I}} - v_{yi}X_i^{\mathrm{I}})]^{\mathrm{T}}$ and $\mathrm{H}_i = [v_{zi}, 0, -v_{xi}, (v_{xi}Z_i^{\mathrm{I}} - v_{zi}X_i^{\mathrm{I}})]^{\mathrm{T}}$.

The Plücker coordinates of the perpendicular line are given as:

$$\mathbb{L}_i = \{(l_i)_{12}, (l_i)_{13}, (l_i)_{14}, (l_i)_{23}, (l_i)_{42}, (l_i)_{34}\} \tag{14}$$

where $(l_i)_{12} = v_x(v_xY_i^{\mathrm{I}} - v_yX_i^{\mathrm{I}})$, $(l_i)_{13} = v_x(v_xZ_i^{\mathrm{I}} - v_zX_i^{\mathrm{I}})$, $(l_i)_{14} = v_x^2$, $(l_i)_{23} = v_xv_zY_i^{\mathrm{I}} - v_xv_yZ_i^{\mathrm{I}}$, $(l_i)_{42} = -v_xv_y$, $(l_i)_{34} = v_xv_z$.

As the perpendicular line $\mathbb{L}_i$ intersects the two lines $\mathbb{L}_i^{\mathrm{I}}$ and $\mathbb{L}_i^{\mathrm{II}}$, the bilinear products of the Plücker coordinates satisfy:

$$\begin{aligned} (\mathbb{L}_i|\mathbb{L}_i^{\mathrm{I}}) = {} & (l_i)_{12}(l_i)_{34}^{\mathrm{I}} + (l_i)_{12}^{\mathrm{I}}(l_i)_{34} + (l_i)_{13}(l_i)_{42}^{\mathrm{I}} \\ & + (l_i)_{13}^{\mathrm{I}}(l_i)_{42} + (l_i)_{14}(l_i)_{23}^{\mathrm{I}} + (l_i)_{14}^{\mathrm{I}}(l_i)_{23} = 0 \end{aligned} \tag{15}$$

$$\begin{aligned} (\mathbb{L}_i|\mathbb{L}_i^{\mathrm{II}}) = {} & (l_i)_{12}(l_i)_{34}^{\mathrm{II}} + (l_i)_{12}^{\mathrm{II}}(l_i)_{34} + (l_i)_{13}(l_i)_{42}^{\mathrm{II}} \\ & + (l_i)_{13}^{\mathrm{II}}(l_i)_{42} + (l_i)_{14}(l_i)_{23}^{\mathrm{II}} + (l_i)_{14}^{\mathrm{II}}(l_i)_{23} = 0 \end{aligned} \tag{16}$$

Stacking Eqs. (7), (8), (14), (15) and (16), we have:

$$\begin{aligned} & -\left[v_xv_y(l_i)_{34}^{\mathrm{I}} + v_xv_z(l_i)_{42}^{\mathrm{I}}\right]X_i^{\mathrm{I}} + \left[v_x^2(l_i)_{34}^{\mathrm{I}} - v_xv_z(l_i)_{14}^{\mathrm{I}}\right]Y_i^{\mathrm{I}} \\ & + \left[v_x^2(l_i)_{42}^{\mathrm{I}} + v_xv_y(l_i)_{14}^{\mathrm{I}}\right]Z_i^{\mathrm{I}} + v_xv_z(l_i)_{12}^{\mathrm{I}} - v_xv_y(l_i)_{13}^{\mathrm{I}} \\ & \qquad + v_x^2(l_i)_{23}^{\mathrm{I}} = 0 \end{aligned} \tag{17}$$

$$\begin{aligned} & -\left[v_xv_y(l_i)_{34}^{\mathrm{II}} + v_xv_z(l_i)_{42}^{\mathrm{II}}\right]X_i^{\mathrm{II}} + \left[v_x^2(l_i)_{34}^{\mathrm{II}} - v_xv_z(l_i)_{14}^{\mathrm{II}}\right]Y_i^{\mathrm{II}} \\ & + \left[v_x^2(l_i)_{42}^{\mathrm{II}} + v_xv_y(l_i)_{14}^{\mathrm{II}}\right]Z_i^{\mathrm{II}} + v_xv_z(l_i)_{12}^{\mathrm{II}} \\ & \qquad - v_xv_y(l_i)_{13}^{\mathrm{II}} + v_x^2(l_i)_{23}^{\mathrm{II}} = 0 \end{aligned} \tag{18}$$

From Eqs. (3), (4), (17) and (18), the two end points of the perpendicular line segment of the two projection lines are solved by the Cramer's Rule as:

$$\mathbf{X}_i^{\mathrm{I}} = \left[\det\left(D_i^{\mathrm{I}}\right)_1 / \det D_i^{\mathrm{I}}, \det\left(D_i^{\mathrm{I}}\right)_2 / \det D_i^{\mathrm{I}}, \det\left(D_i^{\mathrm{I}}\right)_3 / \det D_i^{\mathrm{I}}, 1\right]^{\mathrm{T}} \tag{19}$$

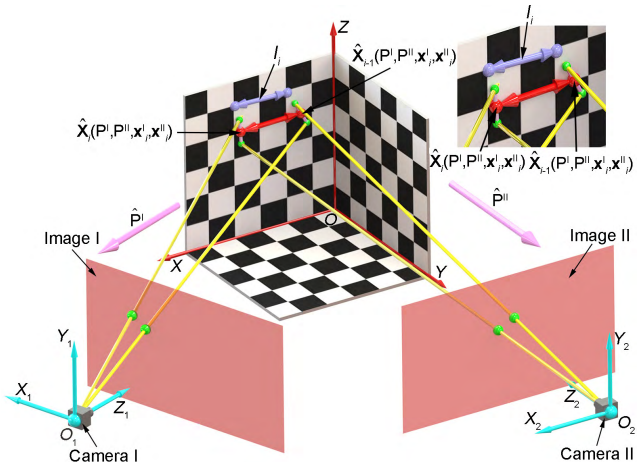

FIGURE 2. Parameterization method of the distance objective generated from two pairs of skew projection lines.

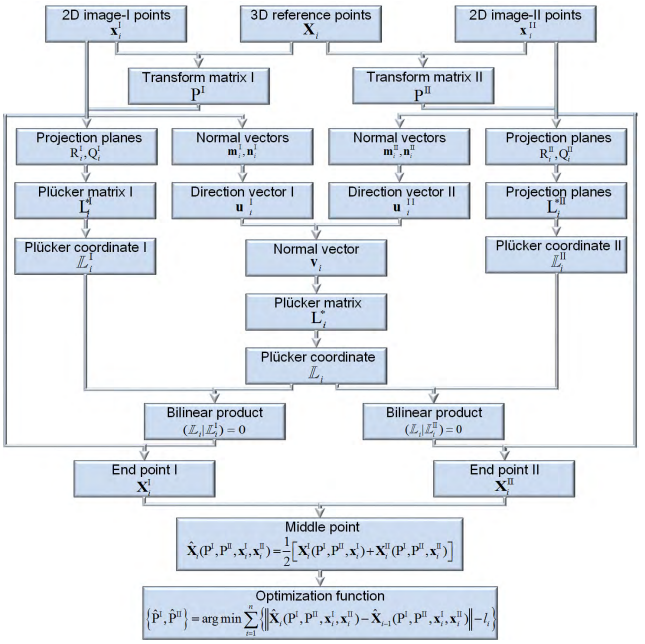

FIGURE 3. Optimization process with the distance objective generated from two pairs of skew projection lines.

$$\mathbf{X}_i^{\mathrm{II}} = \left[\det\left(D_i^{\mathrm{II}}\right)_1 / \det D_i^{\mathrm{II}}, \det\left(D_i^{\mathrm{II}}\right)_2 / \det D_i^{\mathrm{II}}, \det\left(D_i^{\mathrm{II}}\right)_3 / \det D_i^{\mathrm{II}}, 1\right]^{\mathrm{T}} \tag{20}$$

where D_i^{I} and D_i^{II} are the coefficient matrices of Eqs. (3), (17) and Eqs. (4), (18), respectively. $(D_i^{\mathrm{I}})_j$ and $(D_i^{\mathrm{II}})_j$ are the matrices formed by replacing the j-th columns of D_i^{I} and D_i^{II} by the constant column vectors.

As the middle point of the perpendicular line segment is a reasonable estimation of the 3D point [28], the 3D point derived from the 2D projection points $\mathbf{x}_i^{\mathrm{I}}, \mathbf{x}_i^{\mathrm{II}}$, is parameterized as:

$$\hat{\mathbf{X}}_i(\mathrm{P}^{\mathrm{I}}, \mathrm{P}^{\mathrm{II}}, \mathbf{x}_i^{\mathrm{I}}, \mathbf{x}_i^{\mathrm{II}}) = \frac{1}{2}\left[\mathbf{X}_i^{\mathrm{I}}(\mathrm{P}^{\mathrm{I}}, \mathrm{P}^{\mathrm{II}}, \mathbf{x}_i^{\mathrm{I}}) + \mathbf{X}_i^{\mathrm{II}}(\mathrm{P}^{\mathrm{I}}, \mathrm{P}^{\mathrm{II}}, \mathbf{x}_i^{\mathrm{II}})\right] \tag{21}$$

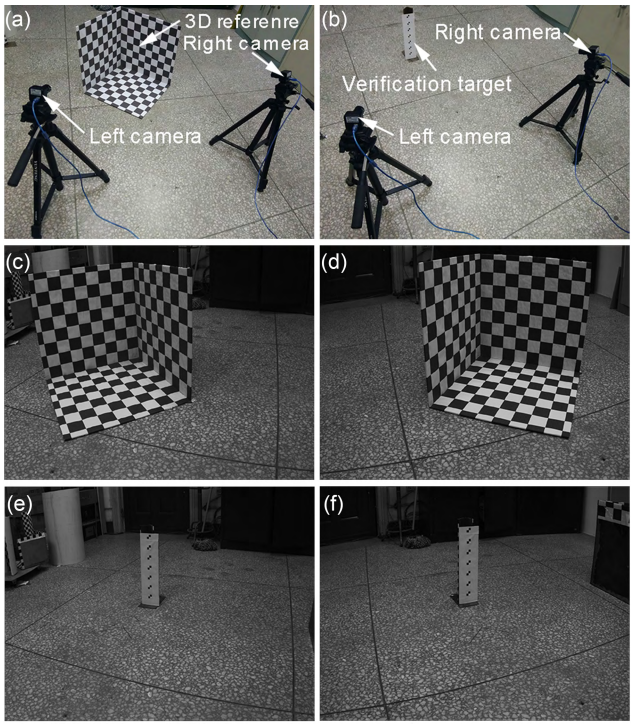

FIGURE 4. Reconstruction and verification experiments of the binocular vision system. (a) Reconstruction setup with a 3D reference, a left camera and a right camera, (b) Verification setup with a target and two cameras, (c) Reconstruction image captured from the right camera, (d) Reconstruction image captured from the left camera, (e) Verification image captured from the right camera, (f) Verification image captured from the left camera.

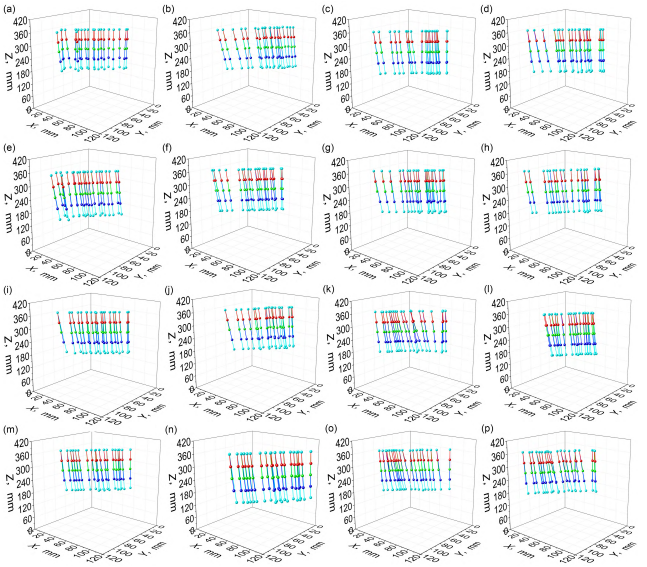

FIGURE 5. Reconstruction results of the benchmark lengths on the target. MD=Measurement Distance, mm, BD=Baseline Distance, mm. (a) MD=900, BD=900, (b) MD=1000, BD=900, (c) MD=1100, BD=900, (d) MD=1200, BD=900, (e) MD=900, BD=1000, (f) MD=1000, BD=1000, (g) MD=1100, BD=1000, (h) MD=1200, BD=1000, (i) MD=900, BD=1100, (j) MD=1000, BD=1100, (k) MD=1100, BD=1100, (l) MD=1200, BD=1100, (m) MD=900, BD=1200, (n) MD=1000, BD=1200, (o) MD=1100, BD=1200, (p) MD=1200, BD=1200.

where $\hat{\mathbf{X}}_i(\mathrm{P}^{\mathrm{I}}, \mathrm{P}^{\mathrm{II}}, \mathbf{x}_i^{\mathrm{I}}, \mathbf{x}_i^{\mathrm{II}})$ is the parameterized estimation on the 3D corner point of the 3D reference. Eq. (21) gives the function relationship between the parameterized 3D corner point and the two projection matrices.

In order to improve the accuracy of the binocular vision measurement, a cost function is constructed to minimize the distance error between the reconstruction points on the 3D reference, as shown in Fig. 2 and Fig. 3. The function with respect to the projection matrices P^{I}, P^{II} is:

$$\left\{\hat{\mathrm{P}}^{\mathrm{I}}, \hat{\mathrm{P}}^{\mathrm{II}}\right\} = \arg\min \sum_{i=1}^{n} \left\{ \left\| \hat{\mathbf{X}}_i(\mathrm{P}^{\mathrm{I}}, \mathrm{P}^{\mathrm{II}}, \mathbf{x}_i^{\mathrm{I}}, \mathbf{x}_i^{\mathrm{II}}) - \hat{\mathbf{X}}_{i-1}(\mathrm{P}^{\mathrm{I}}, \mathrm{P}^{\mathrm{II}}, \mathbf{x}_i^{\mathrm{I}}, \mathbf{x}_i^{\mathrm{II}}) \right\| - l_i \right\} \tag{22}$$

where $\left\{\hat{\mathrm{P}}^{\mathrm{I}}, \hat{\mathrm{P}}^{\mathrm{II}}\right\}$ are the optimization results of the projection matrices. l_i is the standard distance between the adjacent corner points on the 3D reference. The 3D point is reconstructed by $\left\{\hat{\mathrm{P}}^{\mathrm{I}}, \hat{\mathrm{P}}^{\mathrm{II}}\right\}$ and Eqs. (1), (2).

III. RECONSTRUCTION METHOD

3D reconstruction of the binocular vision adopting the distance objective generated from two pairs of skew projection lines is verified by the experiments. The 3D reconstruction method employing the 3D reference in Ref [16] is selected as the comparison method. A target is designed as the benchmark of the reconstruction test. The test lengths of 50 mm, 100 mm, 150 mm and 200 mm are marked by the five collinear feature points on the target. A binocular system with two cameras is built for the verification experiments. The image resolution is 2048 × 1536 in the experiments. The distance between the two cameras is the baseline distance, which contains four cases of 900 mm, 1000 mm, 1100 mm and 1200 mm. The distance between the two cameras and the 3D reference is the measurement distance, which also includes the above four cases. Therefore, sixteen different cases, including four different measurement distances and four different baseline distances, are performed to verify the proposed method. The reconstruction and verification experiments of the binocular vision system are shown in Fig. 4.

Calibration results of the five feature points on the target are shown in Fig. 5. Each subfigure demonstrates the reconstruction results of twenty groups of five feature points on the target. The benchmark lengths of 50 mm, 100 mm, 150 mm and 200 mm are derived from the five uniformly-spaced points. The reconstruction five points are collinear and in the right places relative to the world coordinate system on the 3D calibration reference. The observed distance between two neighbor points is the same as the other distance.

In order to quantitatively evaluate the accuracy of the reconstruction method and compare the distance-

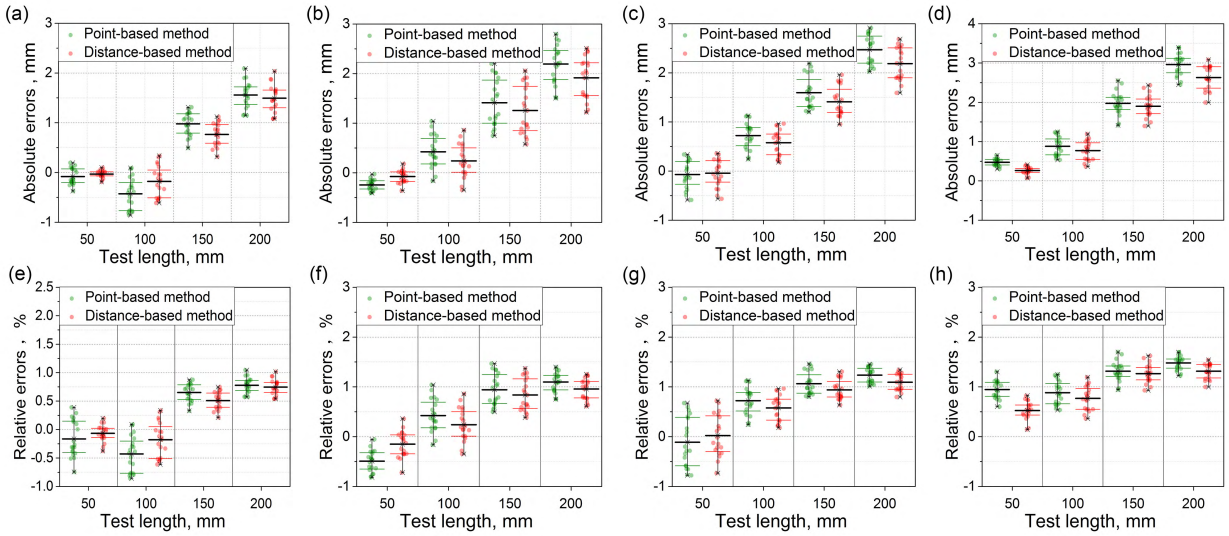

FIGURE 6. Absolute errors and relative errors of the reconstructed test lengths of the distance-based method and point-based method, which relate to Fig. 5(a)-5(d).

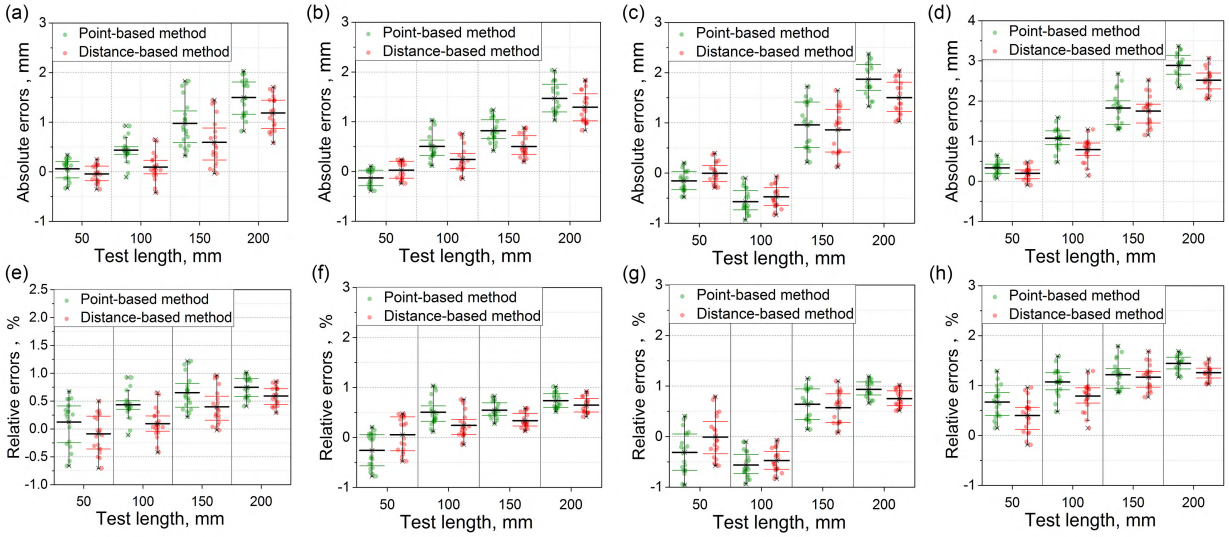

FIGURE 7. Absolute errors and relative errors of the reconstructed test lengths of the distance-based method and point-based method, which relate to Fig. 5(e)-5(h).

based method with the previous point-based method, the absolute errors and the relative errors of the reconstruction lengths on the target are shown in Figs. 6-9, under different baseline distances and different measurement distances. The statistical data are summarized in Table 1.

The experiment results with the increasing test length are explained in Table II. When the baseline distance is 900 mm and the test lengths are 50 mm, 100 mm, 150 mm 200 mm, the root mean squares of the point-based method are 0.32 mm, 0.70 mm, 1.60 mm and 2.37 mm. The root mean squares of the distance-based method are 0.21 mm, 0.54 mm, 1.46 mm and 2.12 mm. For the baseline distance of 1000 mm and the increasing test lengths, the root mean squares of the point-based method are 0.28 mm, 0.74 mm, 1.28 mm and 2.04 mm. The root mean squares of the distance-based method are 0.21 mm, 0.55 mm, 1.12 mm and1.74 mm. In terms of the baseline distance of 1100 mm, the related root mean squares of the point-based method are 0.26 mm, 0.59 mm, 1.21 mm and 1.99 mm. The related root mean squares of the distance-based method are 0.17 mm, 0.46 mm, 0.99 mm and 1.65 mm. With respect to the baseline distance of 1200 mm, the corresponding root mean squares of the point-based method are 0.27 mm, 0.49 mm, 1.00 mm and 1.71 mm. The corresponding root mean squares of distance-based method are 0.21 mm, 0.39 mm, 0.83 mm and 1.35 mm. Thus, the reconstruction

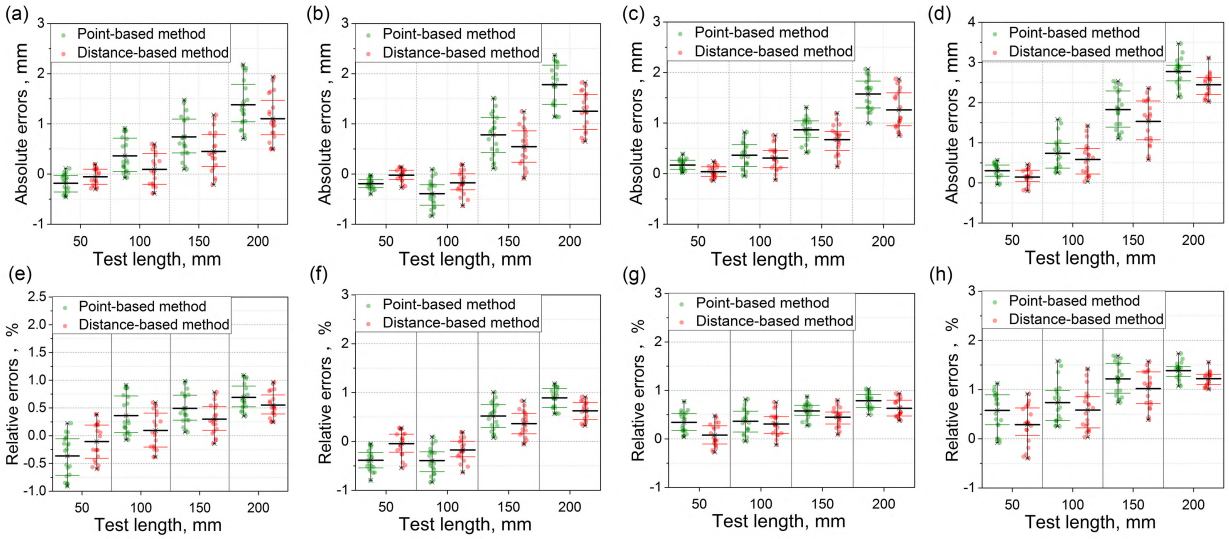

FIGURE 8. Absolute errors and relative errors of the reconstructed test lengths of the distance-based method and point-based method, which relate to Fig. 5(i)-5(l).

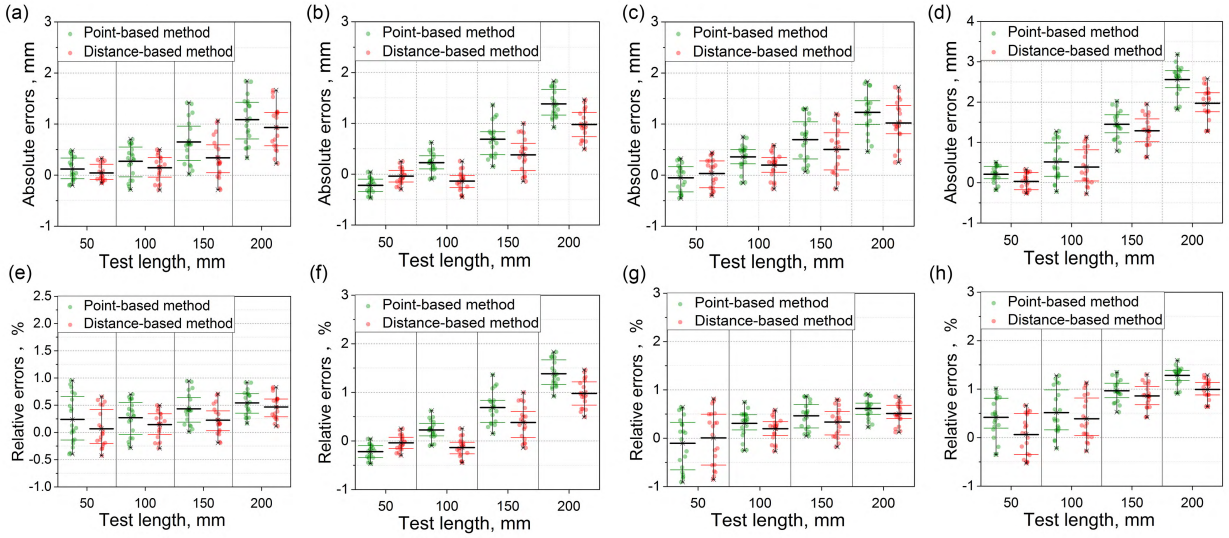

FIGURE 9. Absolute errors and relative errors of the reconstructed test lengths of the distance-based method and point-based method, which relate to Fig. 5(m)-5(p).

error increases with the grow-up test lengths from 50 mm to 200 mm.

The experiment results with the increasing measurement distance are interpreted in Table III. While the baseline distance is 900 mm, the root mean squares of the point-based method are 0.97 mm, 1.37 mm, 1.58 mm and 1.86 mm corresponding to the measurement distances of 900 mm, 1000 mm, 1100 mm and 1200 mm. The root mean squares of the distance-based method are 0.87 mm, 1.20 mm, 1.39 mm and 1.69 mm. When the baseline distance increases to 1000 mm, the root mean squares of the point-based method are 0.97 mm, 0.91 mm, 1.14 mm and 1.82 mm, under the measurement distances of 900 mm, 1000 mm, 1100 mm and 1200 mm. The root mean squares of the distance-based method are 0.73 mm, 0.74 mm, 0.95 mm and 1.61 mm. For the baseline distance of 1100 mm and the same measurement distances, the corresponding root mean squares of the point-based method are 0.89 mm, 0.95 mm, 1.05 mm and 1.74 mm. The root mean squares of the distance-based method are 0.69 mm, 0.75 mm, 0.77 mm and 1.52 mm. Finally, when the baseline distance increases to 1200 mm, the root mean squares of the point-based method are 0.75 mm, 0.80 mm, 0.82 mm and 1.53 mm and the root mean squares of the distance-based method are 0.60 mm, 0.58 mm, 0.67 mm and 1.24 mm. The maximum relative error is 1.48%, which is less than 1.5 %, on the condition that the measurement distance is 1200 mm and

TABLE 1. Experiment results of the verification experiments. Abs is the abbreviation of the absolute error. Rel is the abbreviation of the relative error.

Baseline distance, mm	Method	Measurement distance, mm	Test length, mm							
			50		100		150		200	
			Abs, mm	Rel, %	Abs, mm	Rel, %	Abs, mm	Rel, %	Abs, mm	Rel, %
900	Point-based method	900	0.18	0.35	0.50	0.52	1.01	0.67	1.58	0.79
		1000	0.26	0.53	0.52	0.53	1.48	0.99	2.22	1.11
		1100	0.28	0.49	0.70	0.76	1.74	1.16	2.49	1.25
		1200	0.48	0.96	0.89	0.91	1.99	1.32	2.97	1.48
	Distance-based method	900	0.08	0.15	0.33	0.35	0.79	0.53	1.52	0.76
		1000	0.15	0.29	0.37	0.39	1.34	0.89	1.95	0.98
		1100	0.27	0.40	0.60	0.62	1.55	1.03	2.20	1.10
		1200	0.27	0.55	0.77	0.80	1.91	1.27	2.64	1.32
1000	Point-based method	900	0.21	0.41	0.48	0.50	1.07	0.71	1.54	0.77
		1000	0.21	0.42	0.53	0.56	0.85	0.56	1.50	0.75
		1100	0.28	0.56	0.62	0.63	1.06	0.70	1.89	0.94
		1200	0.36	0.73	1.07	1.10	1.86	1.24	2.90	1.45
	Distance-based method	900	0.17	0.34	0.25	0.27	0.75	0.50	1.23	0.61
		1000	0.17	0.34	0.33	0.35	0.54	0.36	1.32	0.66
		1100	0.22	0.44	0.52	0.54	0.96	0.64	1.53	0.76
		1200	0.25	0.51	0.80	0.83	1.78	1.19	2.53	1.26
1100	Point-based method	900	0.25	0.51	0.47	0.49	0.84	0.56	1.45	0.72
		1000	0.21	0.43	0.44	0.47	0.88	0.58	1.82	0.91
		1100	0.20	0.40	0.42	0.44	0.89	0.59	1.60	0.80
		1200	0.35	0.69	0.80	0.83	1.88	1.25	2.79	1.39
	Distance-based method	900	0.17	0.34	0.32	0.33	0.59	0.39	1.18	0.59
		1000	0.12	0.25	0.26	0.28	0.66	0.44	1.30	0.65
		1100	0.11	0.23	0.34	0.38	0.72	0.48	1.31	0.65
		1200	0.23	0.47	0.68	0.70	1.62	1.08	2.46	1.23
1200	Point-based method	900	0.25	0.51	0.48	0.51	0.76	0.51	1.17	0.58
		1000	0.26	0.53	0.28	0.29	0.75	0.50	1.40	0.70
		1100	0.26	0.53	0.38	0.40	0.80	0.53	1.29	0.64
		1200	0.29	0.58	0.68	0.69	1.48	0.99	2.58	1.29
	Distance-based method	900	0.19	0.38	0.33	0.35	0.50	0.33	1.02	0.51
		1000	0.15	0.31	0.20	0.22	0.50	0.33	1.01	0.50
		1100	0.27	0.55	0.26	0.30	0.66	0.44	1.10	0.55
		1200	0.20	0.40	0.55	0.58	1.33	0.89	2.00	1.01

TABLE 2. Experiment results with different test length. Abs is the abbreviation of the absolute error.

Method	Baseline distance, mm	Test length, mm			
		50	100	150	200
		Abs, mm	Abs, mm	Abs, mm	Abs, mm
Point-based method	900	0.32	0.70	1.60	2.37
	1000	0.28	0.74	1.28	2.04
	1100	0.26	0.59	1.21	1.99
	1200	0.27	0.49	1.00	1.71
Distance-based method	900	0.21	0.54	1.46	2.12
	1000	0.21	0.55	1.12	1.74
	1100	0.17	0.46	0.99	1.65
	1200	0.21	0.39	0.83	1.35

TABLE 3. Experiment results with different measurement distance. Abs is the abbreviation of the absolute error.

Method	Baseline distance, mm	Measurement distance, mm			
		900	1000	1100	1200
		Abs, mm	Abs, mm	Abs, mm	Abs, mm
Point-based method	900	0.97	1.37	1.58	1.86
	1000	0.97	0.91	1.14	1.80
	1100	0.89	0.95	1.05	1.74
	1200	0.75	0.80	0.82	1.53
Distance-based method	900	0.87	1.20	1.39	1.69
	1000	0.73	0.74	0.95	1.61
	1100	0.69	0.70	0.77	1.52
	1200	0.60	0.58	0.67	1.24

the baseline distance is 900 mm. The distance-based method contributes the 27.19%, 38.29%, 19.01%, 16.31% descents for the test lengths of 50mm, 100 mm, 150 mm, 200 mm, compared with the point-based method. As the baseline distance increases from 900 mm to 1200 mm, in most cases, the absolute errors of the reconstructed test lengths show the decreasing trends. When the baseline distance is considered as a constant, the absolute errors of the reconstructed test lengths increase with the measurement distances from 900 mm to 1200 mm.

IV. CONCLUSION

In summary, a 3D reconstruction method for the binocular vision is achieved by the distance objective generated from two pairs of skew projection lines. The end points of the line segment perpendicular to the pair of two projection lines are deduced by the bilinear products among the Plücker coordinates of the projection lines and the line segment. The distance between two feature points on the 3D reference is parameterized by the projection matrices. The cost function is constructed by the difference between the reconstruction distance of the parameterized points and the real distance

on the reference. The measurement distance, the baseline distance and the test length are considered as the accuracy impact factors of the reconstruction method. The baseline distance, as well as the measurement distance includes four cases of 900 mm, 1000 mm, 1100 mm and 1200 mm. The average root mean squares of the distance-based method in the above cases are 0.20 mm, 0.49 mm, 1.12 mm and 1.73 mm when the test length are 50 mm, 100 mm, 150 mm and 200 mm, respectively. The reconstruction error decreases with the increasing baseline distance and the decreasing measurement distance. The comparison experiments prove that the reconstruction method improves the reconstruction accuracy of the binocular vision system.

REFERENCES

[1] Y. Cai, Z. Liu, H. Wang, and X. Sun, "Saliency-based pedestrian detection in far infrared images," *IEEE Access*, vol. 5, pp. 5013–5019, 2017.
[2] A. Glowacz and Z. Glowacz, "Diagnostics of stator faults of the single-phase induction motor using thermal images, MoASoS and selected classifiers," *Measurement*, vol. 93, pp. 86–93, Nov. 2016.
[3] I. Frollo, A. Krafčík, A. P. Andris, J. Přibil, and T. Dermek, "Circular samples as objects for magnetic resonance imaging—Mathematical simulation, experimental results," *Meas. Sci. Rev.*, vol. 15, no. 6, pp. 313–318, 2015.
[4] F. Mufti, R. Mahony, and J. Heinzmann, "Robust estimation of planar surfaces using spatio-temporal RANSAC for applications in autonomous vehicle navigation," *Robot. Auto. Syst.*, vol. 60, no. 1, pp. 16–28, 2012.
[5] A. Nubiola and I. A. Bonev, "Absolute calibration of an ABB IRB 1600 robot using a laser tracker," *Robot. Comput.-Integr. Manuf.*, vol. 29, no. 1, pp. 236–245, 2013.
[6] A. Glowacz and Z. Glowacz, "Diagnosis of the three-phase induction motor using thermal imaging," *Infr. Phys. Technol.*, vol. 81, pp. 7–16, Mar. 2017.
[7] H. Yu, J. H. Shen, R. J. Shah, N. Simaan, and K. M. Joos, "Evaluation of microsurgical tasks with OCT-guided and/or robot-assisted ophthalmic forceps," *Biomed. Opt. Exp.*, vol. 6, no. 2, pp. 457–472, 2015.
[8] F. Rottensteiner, G. Sohn, M. Gerke, J. D. Wegner, U. Breitkopf, and J. Jung, "Results of the ISPRS benchmark on urban object detection and 3D building reconstruction," *ISPRS J. Photogramm.*, vol. 93, no. 7, pp. 256–271, 2014.
[9] S. Zhang, D. V. D. Weide, and J. Oliver, "Superfast phase-shifting method for 3-D shape measurement," *Opt. Exp.*, vol. 18, no. 9, pp. 9684–9689, 2010.
[10] F. Qi, Y. Luo, and D. Hu, "Camera calibration with one-dimensional objects moving under gravity," *Pattern Recognit.*, vol. 40, no. 1, pp. 343–345, 2007.
[11] Z. Zhang, "A flexible new technique for camera calibration," *IEEE Trans. Pattern Anal. Mach. Intell.*, vol. 22, no. 11, pp. 1330–1334, Nov. 2000.
[12] C. Yu and Q. Peng, "Robust recognition of checkerboard pattern for camera calibration," *Opt. Eng.*, vol. 45, no. 9, p. 093201, 2006.
[13] J. E. Ha, "Automatic detection of chessboard and its applications," *Opt. Eng.*, vol. 48, no. 6, p. 067205, 2009.
[14] C. Ricolfe-Viala and A.-J. Sánchez-Salmerón, "Robust metric calibration of non-linear camera lens distortion," *Pattern Recognit.*, vol. 43, no. 4, pp. 1688–1699, 2010.
[15] Y. I. Abdel-Aziz and H. M. Karara, "In direct linear transformation into object space coordinates in close-range photogrammetry," in *Proc. Symp. Close-Range Photogram.*, Falls Church, VA, USA, 1971, pp. 1–18.
[16] G. Xu *et al.*, "Three degrees of freedom global calibration method for measurement systems with binocular vision," *J. Opt. Soc. Korea*, vol. 20, no. 1, pp. 107–117, 2016.
[17] C. Ricolfe-Viala and A.-J. Sánchez-Salmerón, "Using the camera pinhole model restrictions to calibrate the lens distortion model," *Opt. Laser Technol.*, vol. 43, no. 6, pp. 996–1005, 2011.
[18] P. Zhang, H. Zhao, X. Zhou, and J. Li, "Sub-aperture stitching interferometry using stereovision positioning technique," *Opt. Exp.*, vol. 18, no. 14, pp. 15216–15222, 2010.
[19] R. Gupta and R. I. Hartley, "Linear pushbroom cameras," *IEEE Trans. Pattern Anal. Mach. Intell.*, vol. 19, no. 9, pp. 963–975, Sep. 1997.
[20] P. Zhao and N. H. Wang, "Precise perimeter measurement for 3D object with a binocular stereo vision measurement system," *Optik*, vol. 121, no. 10, pp. 953–957, 2010.
[21] G. Xu, X. Li, J. Su, H. Pan, and G. Tian, "Precision evaluation of three-dimensional feature points measurement by binocular vision," *J. Opt. Soc. Korea*, vol. 15, no. 1, pp. 30–37, 2011.
[22] D. G. Lowe, "Distinctive image features from scale-invariant keypoints," *Int. J. Comput. Vis.*, vol. 60, no. 2, pp. 91–110, 2004.
[23] J. Heikkila, "Geometric camera calibration using circular control points," *IEEE Trans. Pattern Anal.*, vol. 22, no. 10, pp. 1066–1077, Oct. 2000.
[24] L. G. Shapiro and G. C. Stockman, *Computer Vision*. Englewood Cliffs, NJ, USA: Prentice-Hall, 2001.
[25] Y. I. Abdel-Aziz, H. M. Karara, and M. Hauck, "Direct linear transformation from comparator coordinates into object space coordinates in close-range photogrammetry," *Photogramm. Eng., Remote Sens.*, vol. 81, no. 2, pp. 103–107, 2015.
[26] R. Hartley and A. Zisserman, *Multiple View Geometry in Computer Vision*. Cambridge, U.K.: Cambridge Univ. Press, 2003.
[27] D. C. Lay, *Linear Algebra and Its Applications*. Reading, MA, USA: Addison-Wesley, 2003.
[28] Q. Wang, Z. Wang, Z. Yao, J. Forrest, and W. Zhou, "An improved measurement model of binocular vision using geometrical approximation," *Meas. Sci. Technol.*, vol. 27, no. 12, p. 125013, 2017.

GUAN XU was born in Changchun, China, in 1981. He received the B.S., M.S., and Ph.D. degrees in vehicle operation engineering from Jilin University, Jilin, China, in 2003, 2006, and 2009, respectively. His research interests include active vision and binocular vision in vehicle inspection techniques.

JUNYI CHEN was born in Jilin, China, in 1995. She received the B.S. degree in vehicle operation engineering from Jilin University, Jilin, China, in 2017. Her research interest includes active vision and binocular vision in vehicle inspection techniques.

XIAOTAO LI was born in Changchun, China, in 1980. She received the B.S., M.S., and Ph.D. degrees in mechanical engineering from Jilin University, Jilin, China, in 2010. Her research interest includes vision-based measurement and MEMS.